Journal of Propulsion and Power
Vol. 12, No. 1, January–February 1996

Influence of Rocket Design Parameters on Engine Nozzle Efficiencies

Detlef Manski* and Gerald Hagemann*
DLR, German Aerospace Research Establishment, D-74239 Lampoldshausen, Germany

This article presents results of flow calculations of large H_2/O_2 rocket nozzles, using a modified version of JANNAF's two-dimensional kinetic program. Various calculations of rocket nozzles were performed to study the influence of characteristic rocket engine design parameters on nozzles losses. The domain of nozzle losses is classified by divergence, friction, and kinetics. In addition, the influence of shocks in the nozzle and cooling effects on the efficiencies have been considered. The losses are determined using nozzle shapes of the Space Shuttle main engine and Vulcan HM60 engines, which are characteristic for future rocket launchers. The rocket design parameters are parametrically derived vs thrust, chamber pressure, mixture ratio, nozzle area ratio, and nozzle geometry. All of these parameters are systematically varied and their effects on nozzle efficiencies are presented.

Nomenclature

c = velocity
c_F = thrust coefficient, I_s/c^*
c^* = characteristic velocity, $p_cA_t/\dot{m}$
I = impulse
p = pressure
r = mass ratio oxidizer/fuel mixture
T = temperature
α = angle
δ = displacement thickness
ε = nozzle area ratio
η = efficiency
θ = momentum thickness
ρ = density

Subscripts
a = ambient
ad = adaptive
c = combustion chamber
comp = combustion
div = divergence, two dimensionality
e = exit
eff = effective
fric = friction, boundary layer
hl = heat loss
noz = nozzle
s = specific
stoi = stoichiometric
t = throat
vac = vacuum
w = wall

Introduction

THE calculated engine nozzle efficiencies are stored in a database for system analyses of future rocket launchers,[1] where nozzle flows are simulated under simplified assumptions such as one-dimensional, isentropic ideal gas flows. The database will be used to modify the simplified nozzle flow assumption.

Only a few studies on the dependencies of nozzle losses on characteristic nozzle design parameters can be found. In Ref. 2, friction losses of small N_2H_4 engines in the thrust class of F_{vac} = 0.5 kN were examined. Miyajima[3] examined kinetic, friction, and divergence impulse efficiencies of H_2/O_2 rocket nozzles with thrust levels of F_{vac} = 4.0 kN as a function of chamber mixture ratio. Using the simplified procedure of the JANNAF performance methodology, analytical functions were derived[4] for various H_2/O_2 rocket nozzle losses in a thrust level of the RL-10 engine. The results presented in this article give thorough insight into various losses of large liquid rocket engines of the Space Shuttle main engine (SSME) and Vulcan HM60 class engines, and the dependencies of the losses on characteristic nozzle design parameters.

Losses in Thrust Chambers

Thrust chamber losses are caused by imperfect energy release in combustion chambers and imperfect expansion processes in the nozzles. It is necessary to limit the nozzle exit pressure to avoid severe flow separation at the exit of first-stage rocket engine nozzles. This minimum exit pressure can be estimated using the Summerfield[6] criterion. The ideal contour nozzle produces a homogeneous flowfield with a constant velocity distribution in the exit area, but it is too long for application in launchers. Therefore, most of today's rocket nozzles have a length approximately 80% of their ideal length. The contours of shortened nozzles for maximum thrust can be calculated with the method of characteristics as proposed by, e.g., Rao,[5] or can be analytically designed by a method where the throat contours are described by circular arcs and the divergent contours are parabolic. The latter type of nozzles are often called parabolic or Rao nozzles.[6]

Divergence Losses

For both design cases, these nonideal bell-shaped nozzles produce nonuniform pressure and velocity profiles in the exit plane. The losses due to these inhomogeneous exit flowfields are considered here as two-dimensional or divergence losses. They also include losses induced by shock waves emanating from the throat region of nonideal nozzle contours.

Friction and Heat Flux Losses

Further losses are caused by viscous effects in boundary layers and by heat transfer from the main flow to the nozzle

Received May 5, 1994; presented as Paper 94-2756 at the AIAA/ASME/SAE/ASEE 30th Joint Propulsion Conference, Indianapolis, IN, June 27–29, 1994; revision received March 17, 1995; accepted for publication April 19, 1995.

*Aerospace Engineer, Institute for Chemical Propulsion and Engineering. Member AIAA.

wall. These losses strongly depend on the nozzle size and heat fluxes across the wall.

Kinetic Losses

Because of the high temperature of the combustion process in the rocket chamber, dissociation takes place. During the nozzle expansion process, the static temperature decreases and causes the gas to seek new equilibrium states with lower degrees of dissociation. However, this requires time, so that the fluid may not obtain new equilibrium states, resulting in nonequilibrium, and finally, in frozen flow in which all recombinations are suppressed during expansion. That means that the energy stored in dissociation products cannot be released. These losses are called kinetic losses.

Combustion Chamber Losses

Losses due to imperfections in vaporization, mixing, and combustion in the combustion chamber are not examined in this article. Thus, a homogeneous inflow with an average mixture ratio is assumed in these numerical simulations.

Following the JANNAF performance methodology, the specific impulse of thrust chambers can be determined from

$$I_{s_{eff}} = (\eta_{I_{s_{comb}}} \cdot \eta_{I_{s_{mix}}} \cdot \eta_{I_{s_{vap}}} \cdot \eta_{I_{s_{kin}}} \cdot \eta_{I_{s_{div}}} \cdot \eta_{I_{s_{fric}}} \cdot \eta_{I_{s_{hl}}}) I_{s_{ODE}} \qquad (1)$$

$I_{s_{eff}}$ is determined by thrust measurement. The specific impulse $I_{s_{ODE}}$ is calculated by a one-dimensional equilibrium analysis, e.g., by Gordon and McBride,[7] using the average mixture ratio in the combustion chamber. Since losses in the combustion chambers are not the subject in this article, the first three efficiencies, which can be summarized as the efficiency of energy release in the combustion chamber

$$\eta_{c^*} = \eta_{I_{s_{comb}}} \cdot \eta_{I_{s_{mix}}} \cdot \eta_{I_{s_{vap}}}$$

are neglected in the succeeding analysis. η_{c^*} values are in the order of 99%. Furthermore, the total radiation of the thrust chamber was assumed to be zero. However, the remaining heat losses across nozzle walls hl, i.e., regenerative cooling, are considered and included in the boundary-layer losses, fric, and therefore, characterized by $\eta_{I_{s_{fric}}}$.

Definition of Efficiencies in Rocket Nozzles

The influence of losses in the expansion process was studied as a function of characteristic rocket design parameters. The following losses that were mentioned previously were the subject of the study: 1) losses caused by kinetic effects, 2) divergence losses including losses caused by shocks, and 3) friction and heat flux induced losses.

To characterize the kinetic losses, a kinetic efficiency $\eta_{I_{s_{kin}}}$ is defined as

$$\eta_{I_{s_{kin}}} = I_{s_{ODK}} / I_{s_{ODE}} \qquad (2)$$

with the specific impulse $I_{s_{ODK}}$ calculated by the one-dimensional kinetic flow analysis.

The divergence efficiency $\eta_{I_{s_{div}}}$ is defined as

$$\eta_{I_{s_{div}}} = I_{s_{2D}} / I_{s_{ODK}} \qquad (3)$$

with the specific impulse $I_{s_{2D}}$ calculated by the two-dimensional flow analysis including kinetic effects.

The friction efficiency $\eta_{I_{s_{fric}}}$ is defined as

$$\eta_{I_{s_{fric}}} = I_{s_{BL}} / I_{s_{2D}} \qquad (4)$$

The specific impulse $I_{s_{BL}}$ is calculated by a two-dimensional flow analysis including kinetics, boundary-layer, and heat transfer effects.

The nozzle efficiency $\eta_{I_{s_{noz}}}$ follows from

$$\eta_{I_{s_{noz}}} = \eta_{I_{s_{kin}}} \eta_{I_{s_{div}}} \eta_{I_{s_{fric}}} \qquad (5)$$

Because of the pressure term the efficiencies differ for sea level, vacuum, or altitude adaptive specific impulses. In this article all efficiencies are referred to the specific vacuum impulse.

Numerical Methods

To perform the numerical calculation of the previously defined nozzle efficiencies, the program two-dimensional kinetic (TDK)[8] was used, it is a well-established program for one- and two-dimensional flowfield calculations of rocket nozzles including equilibrium, kinetic, shocks, and boundary-layer effects. TDK was developed for the JANNAF computer program methodology with the aim of theoretical performance prediction of large liquid rocket engines. The program was modified and adapted for the parametric analysis done in this work. The modular structure of TDK is shown in Fig. 1. Further details concerning TDK can be found in Refs. 8 and 9.

To perform parametric studies, TDK was implemented in the system analysis program SYS,[10] which was originally written for the system analysis of space transportation vehicles. Systematic variations of the following characteristic nozzle design parameters were performed: 1) p_c = 25, 50, 100, 200, and 400 bar; 2) $r_t = (i \cdot 2)^{\pm 1/2} \cdot r_{t_{ref}}$, with $r_{t_{ref}}$ = 0.131 m, i = 1, 2, 4, and 8; 3) ε = 45, 77.5, and 126; 4) $\alpha_{w,e} = 0 \div 15$

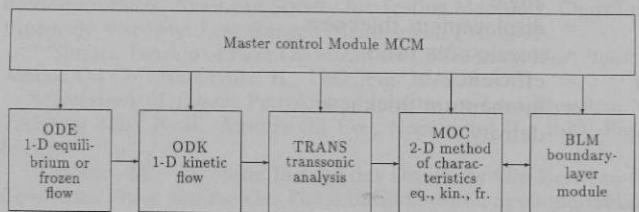

Fig. 1 Modular structure of TDK.

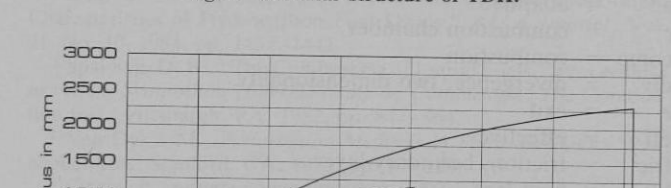

Fig. 2 Contours of SSME nozzles with three different throat radii (r_t = 0.065, 0.13, and 0.26 m).

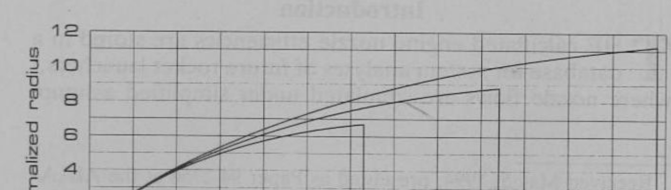

Fig. 3 Contour of the SSME nozzle and nozzles with an area ratio of ε = 45 and 126.

deg; 5) O/F = 4.0, . . . , 9.5; and 6) wall cooling methods = adiabatic, regenerative, and dump cooling.

The nozzles of the SSME and Vulcan engines were taken as reference nozzles. The variation of the throat radius implies a scaling of the whole engine, since all of the geometrical data are normalized by the throat radius. Figure 2 shows nozzle contours for three different throat radii.

Corresponding to the chamber pressures of p_c = 100, 200, and 400 bar, three exit area ratios were chosen under conditions that satisfied the Summerfield criterion to avoid flow separation in the nozzle under sea level conditions. Figure 3 represents the divergent contours of the investigated nozzles with the three area ratios of ε = 45, 77.5, and 126, where the nozzle contour with an area ratio of ε = 45 is equal to the Vulcan nozzle contour.

Nozzle Flowfield Calculations

The SSME nozzle is chosen as a reference. All calculations were performed under consideration of turbulent fluctuations in the boundary-layer and adiabatic wall conditions.

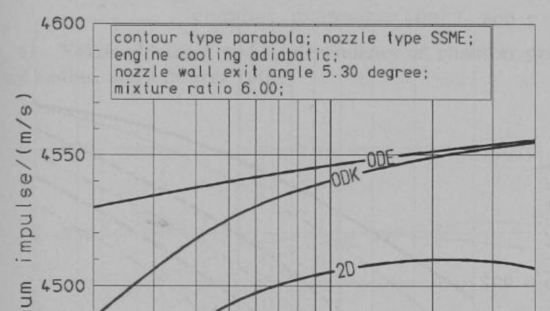

Fig. 4 Different specific impulses as function of chamber pressures.

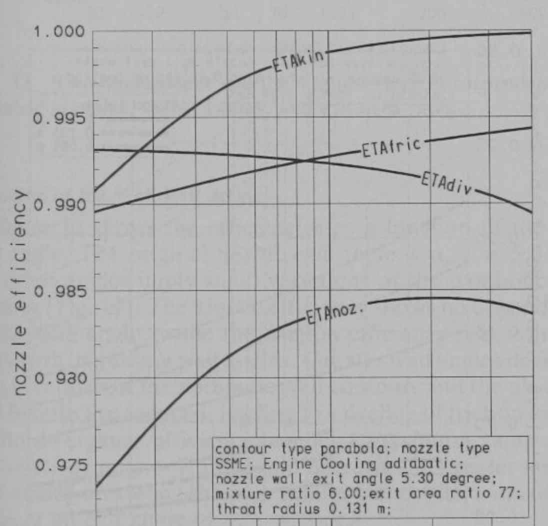

Fig. 5 Different efficiencies as function of chamber pressure.

Tendencies of the Nozzle Losses

The variation of chamber pressure at constant exit area ratio gives a first insight in the order of magnitude of the different specific impulses and efficiencies. With increasing chamber pressure the degree of dissociation in the combustion chamber monotonously decreases, resulting in an increase of specific impulses. Furthermore, effects of kinetics in the nozzle also decrease (compare Figs. 4 and 5). An increase in density due to pressure rise leads to a stronger increase of recombination reactions than that of dissociation reactions.[11,12] The degree of dissociation in the combustion chamber decreases and nonequilibrium effects in the nozzle are reduced, resulting in an increase of the kinetic efficiency. The divergence influence increases with increasing chamber pressure as shown in Fig. 5. It becomes obvious that lower chamber pressure produces a more homogeneous flowfield in the nozzle exit. In contrast, the influence of friction decreases with increasing chamber pressure, which becomes more obvious in subsequent figures.

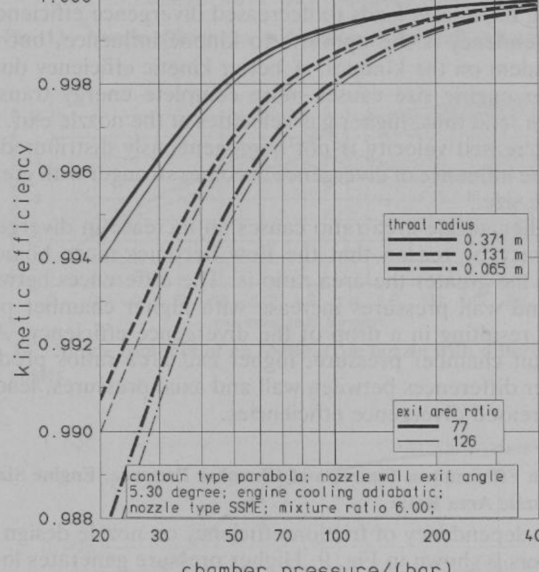

Fig. 6 Kinetic efficiency as function of chamber pressure, engine size, and exit area ratio.

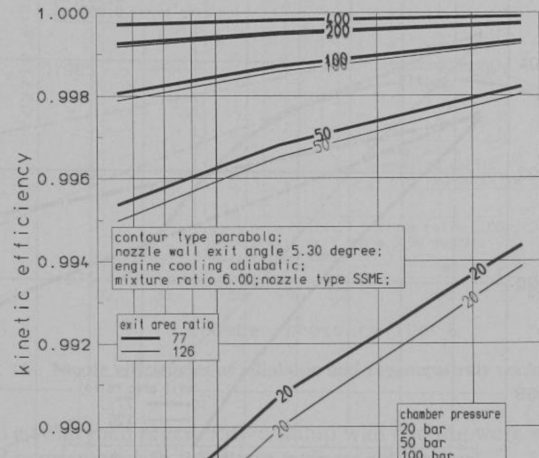

Fig. 7 Kinetic efficiency as function of chamber pressure, engine size, and exit area ratio.

Kinetic Efficiency as Function of Chamber Pressure, Engine Size, and Nozzle Area Ratio

Figures 6 and 7 show the dependency of kinetic efficiency on chamber pressure, engine size, and nozzle exit area ratio. The pressure already discussed has a dominating influence. Second-order influence is given by the size of the engine. The absolute length of the nozzle decreases with reduced throat radius, leading to shorter durations of stay of the fluid in the nozzle. This implies that there is less time for the dissociated particles to recombine, resulting in a decrease of the kinetic efficiency. Higher area ratios cause the kinetic efficiency to decrease slightly, because the longer section of the nozzle is flown through by frozen gas compositions, whereas the zero-point energy of the dissociation products can no longer be transformed. Thus, the difference between equilibrium and kinetic (frozen) solution enhances with higher area ratios, and that amplifies the kinetic effects.

Divergence Efficiency as Function of Chamber Pressure, Engine Size, and Nozzle Area Ratio

Figure 8 shows variations of the divergence efficiency. Enlarging the nozzle leads to decreased divergence efficiencies. This tendency is the opposite to kinetic influence, but it is dependent on the kinetics. A better kinetic efficiency due to greater engine size causes more complete energy transformation, and thus, higher gas velocities at the nozzle exit. But the increased velocity is not homogeneously distributed, so that the influence of divergence becomes stronger with greater engine size.[9]

Higher nozzle area ratio causes an increase in divergence efficiency by reason that the flow becomes more homogeneous the greater the area ratio is. The differences between axis and wall pressures increase with higher chamber pressures, resulting in a drop of the divergence efficiency. At a constant chamber pressure, higher exit area ratios produce smaller differences between wall and axial pressures, leading to increased divergence efficiencies.

Friction Efficiency as Function of Chamber Pressure, Engine Size, and Nozzle Area Ratio

The dependency of friction efficiency on nozzle design parameters is shown in Fig. 9. Higher pressure generates lower boundary-layer thickness (as seen in Fig. 10), and therefore, better friction efficiency. Higher area ratios imply longer walls with increased friction losses, so that the friction efficiency decreases with higher area ratios. Greater engine size increases the nozzle length, and thus, the boundary-layer thickness, but the relative displacement thicknesses normalized with the throat radius decreases (Fig. 10). Therefore, the friction efficiency increases with engine size.

Nozzle Efficiency as Function of Chamber Pressure, Engine Size, and Nozzle Area Ratio

The overall nozzle efficiency is presented in Fig. 11. Increasing friction and kinetic efficiencies with increasing chamber pressures lead to an increase of the nozzle efficiency, before the decreasing divergence efficiencies begin to dominate at higher chamber pressures. The corresponding specific impulses are presented in Fig. 12. The overlay of the previously discussed effects shows that, at low chamber pressures, large engines have a better performance than smaller engines, while at high pressures this tendency is reversed.

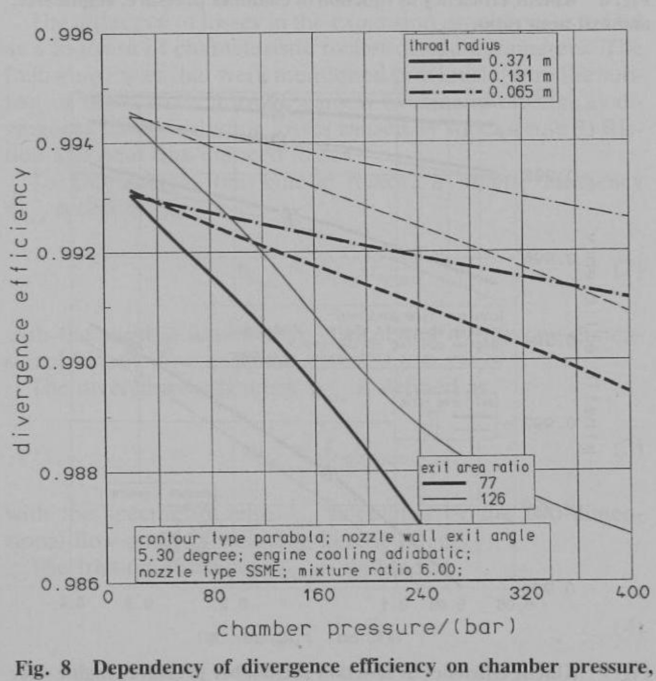

Fig. 8 Dependency of divergence efficiency on chamber pressure, throat radius, and exit area ratio.

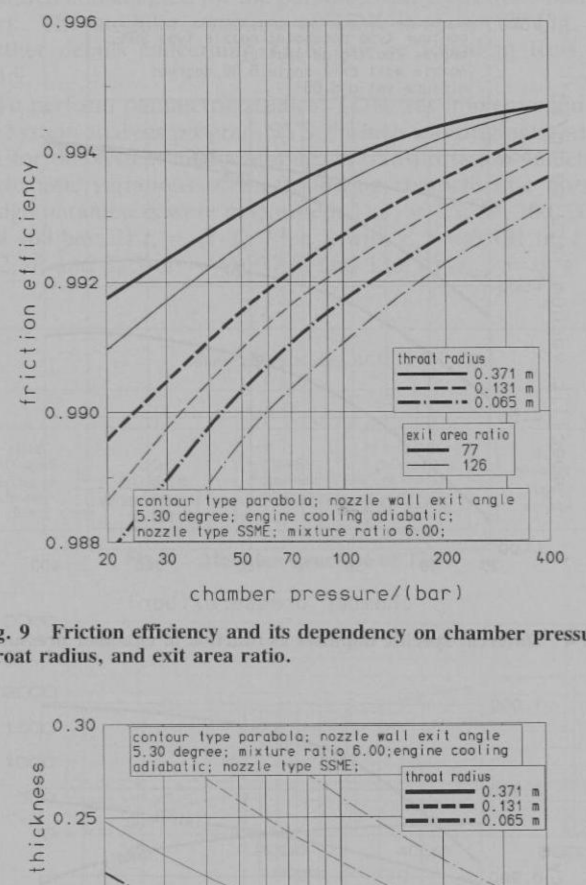

Fig. 9 Friction efficiency and its dependency on chamber pressure, throat radius, and exit area ratio.

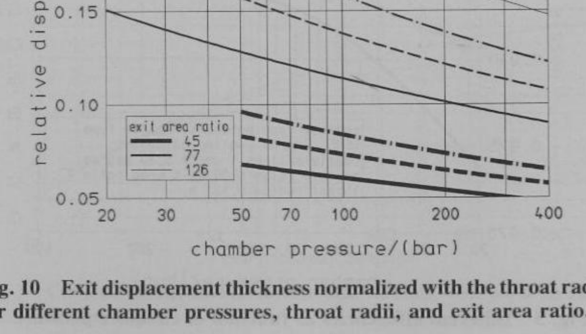

Fig. 10 Exit displacement thickness normalized with the throat radius for different chamber pressures, throat radii, and exit area ratio.

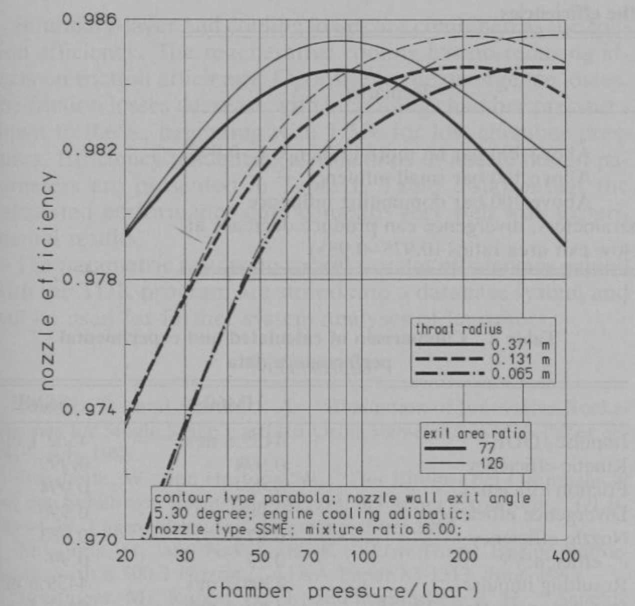

Fig. 11 Nozzle efficiency and its dependency on chamber pressure, throat radius, and exit area ratio.

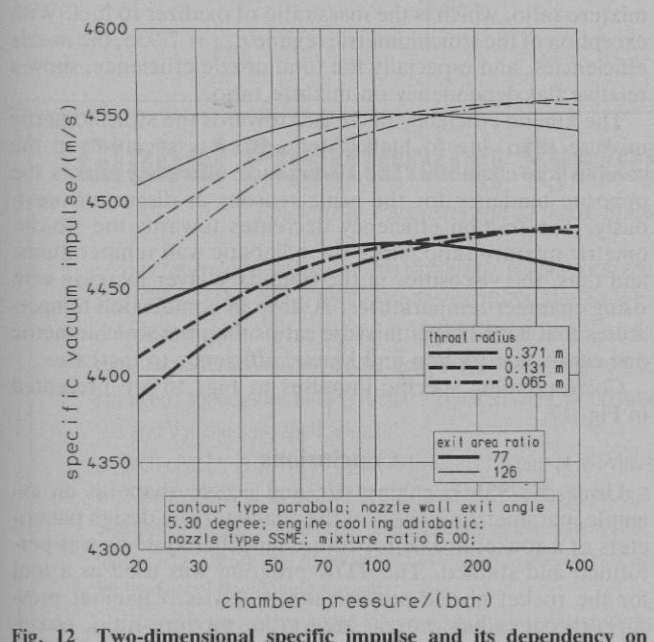

Fig. 12 Two-dimensional specific impulse and its dependency on chamber pressure, throat radius, and exit area ratio.

Variation of the Wall Exit Angle

Figure 13 shows the efficiencies as a function of the wall exit angle. The original SSME exit angle is $\alpha_{w,e} = 5.3$ deg, the other angles imply small variations of the parabolic wall contour (Fig. 14). The kinetic efficiency shows no dependency on the wall angle, while the friction efficiency rises continuously with increasing wall angles. Greater wall angles decrease the curvatures of the parabolic wall contours and the absolute wall lengths are reduced, leading to a decline of friction losses.

The divergence efficiency reaches a maximum value at an exit angle of $\alpha_{w,e} = 7.5$ deg and decreases at greater angles. The nozzle efficiency shows a similar trend with a maximum value at an exit angle of $\alpha_{w,e} = 8$ deg.

Comparison of Adiabatic Walls with Cooled Walls

The influence of cooled nozzle walls on the specific impulses is included in the friction efficiency. Regenerative wall cooling

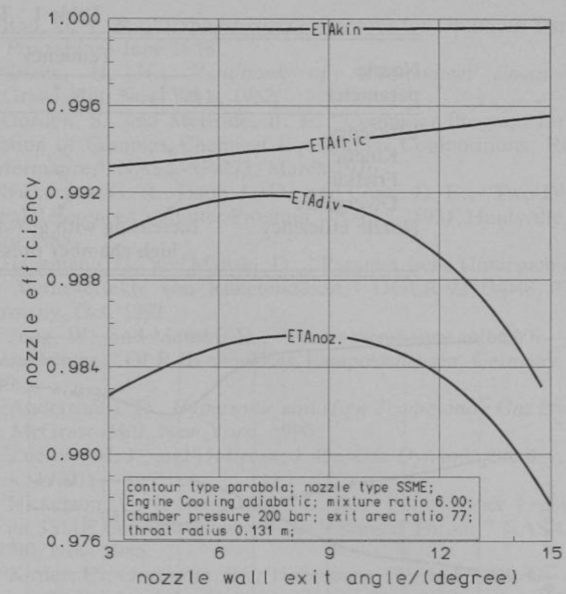

Fig. 13 Nozzle efficiencies as function of the wall exit angle.

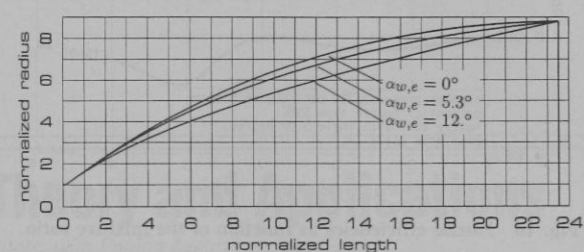

Fig. 14 Nozzle contours of an SSME-type nozzle with different wall exit angles.

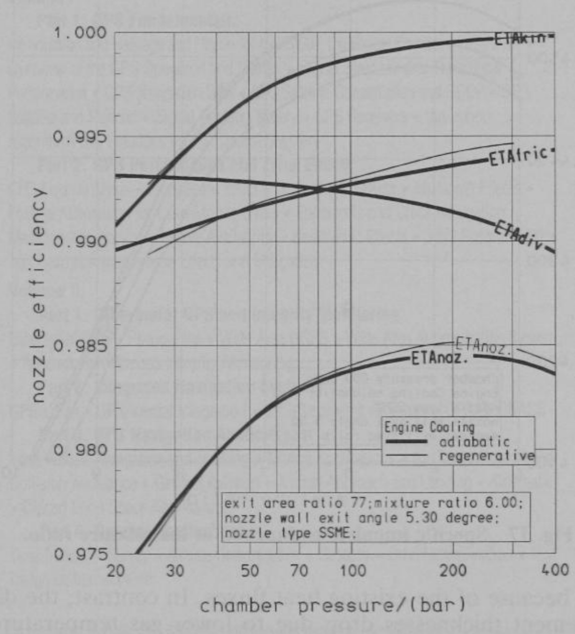

Fig. 15 Nozzle efficiencies at adiabatic and regeneratively cooled walls.

and a combined regenerative/dump wall cooling were studied and compared with adiabatic wall conditions.

TDK calculations of SSME nozzles with an adiabatic wall condition and a fully regeneratively cooled wall showed negligible differences in the resulting specific impulses and in the efficiencies, since the heat fluxes across the wall are transferred to the fuel mass flow (Fig. 15). The momentum thicknesses rise considerably in case of the regeneratively cooled

Table 1 Trends of the efficiencies

Nozzle parameter	Tendency $p_c \uparrow$	$r_t \uparrow$	$\varepsilon_e \uparrow$	Remarks
Efficiency				
Kinetic	↗	↗	↘	Above 100 bar no more influence (>0.995)
Friction	↗	↗	↘	Above 100 bar small influence
Divergence	↘	↘	↗	Above 100 bar dominating influence
Nozzle efficiency	Increasing with growth of all parameters, divergence can produce decrease at high chamber pressures and low exit area ratios (0.975–0.985)			

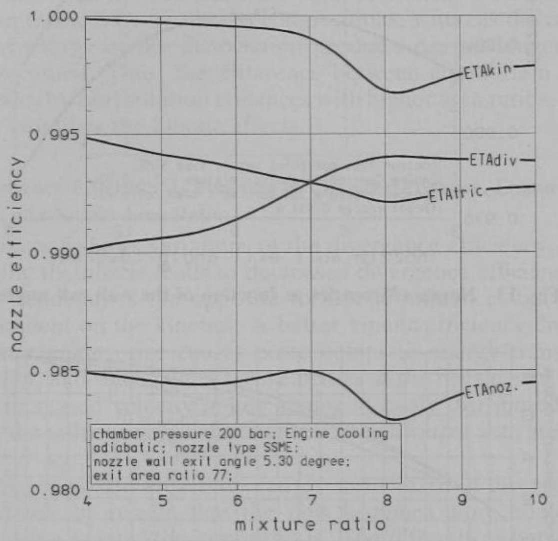

Fig. 16 Nozzle efficiencies as function of the mixture ratio.

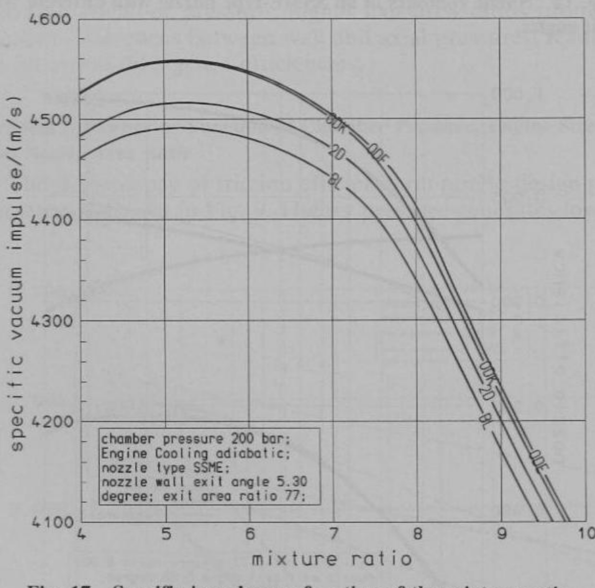

Fig. 17 Specific impulses as function of the mixture ratio.

wall because of the existing heat fluxes. In contrast, the displacement thicknesses drop due to lower gas temperatures compared to the adiabatic wall. In the case of combined regeneratively cooled and dump cooled nozzle walls, as realized in the HM60 engine, a strong decrease in the friction efficiencies can be observed due to the loss of heat across the dump cooled walls. The other efficiencies show no further differences.[9]

Effects of Mixture Ratio Variations

For an engine size and chamber pressure like that of the SSME class, Fig. 16 shows nozzle efficiencies as a function of mixture ratio, which is the mass ratio of oxidizer to fuel. With exception of the stoichiometric regime $r_{stoi} = 7.936$, the nozzle efficiencies, and especially the total nozzle efficiency, show a relative flat dependency on mixture ratio.

Table 2 Comparison of calculated and experimental performance data

	HM60	SSME
Impulse, ODE[7]	4455.8 m/s	4562.1 m/s
Kinetic efficiency	0.998	0.999
Friction efficiency	0.989	0.994
Divergence efficiency	0.988	0.990
Nozzle efficiency	0.977	0.983
c* efficiency[13]	0.99	0.99
Resulting impulse	4309.7 m/s	4439.6 m/s
Impulse, e.g., Refs. 14, 15	4305.1 m/s	4441.4 m/s
Relative error, %	0.1	0.04

The kinetic efficiency decreases towards the stoichiometric mixture ratio due to higher degrees of dissociation in the combustion chamber. The divergence efficiency shows the opposite tendency for the same reasons as discussed previously. The friction efficiency decreases towards the stoichiometric mixture ratio, since the adiabatic wall temperatures, and thus, the viscosities in the boundary layer increase with rising chamber temperatures. A drop in combustion temperatures that have higher mixture ratios than the stoichiometric one causes the friction and kinetic efficiency to increase.

Corresponding specific impulses to Fig. 16 are presented in Fig. 17.

Conclusions

Using the SSME engine size and nozzle shape as an example, parametric analysis of the characteristic design parameters of a rocket nozzle for future launcher systems was performed and studied. The TDK program was used as a tool for the rocket nozzle performance analysis. Chamber pressure, throat radius, nozzle area ratio, mixture ratio, nozzle exit angle, and the nozzle cooling method were used as characteristic nozzle design parameters to study their influence. The nozzle performance parameters were defined and explained.

To describe the total losses of rocket nozzle energy release, the losses were divided into three main effects and characterized with kinetic, divergence, and friction nozzle efficiencies.

It has been shown that the total nozzle efficiency of first-stage hydrogen/oxygen engines for low chamber pressures is in a regime of 97%. For chamber pressures up to 100 bar total nozzle efficiencies of 98% and more are available. In that thrust and chamber pressure regime the total nozzle efficiency remains nearly constant at that value.

The divergence losses due to two-dimensional effects represents the main part of the total nozzle losses. The losses increase with chamber pressures up to 1.5%, beginning at 0.6% for low chamber pressures.

The kinetic losses are nearly zero for chamber pressures higher than 100 bar and thrust levels of the SSME class. At lower chamber pressures, the kinetic losses rise to 1%.

Boundary-layer and cooling losses are combined as the friction efficiency. The regenerative cooling has no reducing effects on friction efficiency. Opposite to the divergence losses, the friction losses decrease with increasing chamber pressures down to 0.6%, beginning with 1.5% for low chamber pressures. Efficiency tendencies as functions of nozzle design parameters are presented in Table 1. Table 2 shows that the calculated performance data compare very well with experimental results.

The parametric results on rocket nozzles efficiencies gained with the TDK program are stored into a database system and will be used for further system analyses of launchers.

References

[1]Manski, D., and Martin, J. A., "Evaluation of Innovative Rocket Engines for Single Stage Earth-to-Orbit Vehicles," AIAA Paper 88-2819, July 1988.

[2]Buschulte, W., and Hartung, W., "Der Einfluss der Grenzschicht auf den Schub von Kleinsttriebwerken bei hoher Expansion," DLR-FB-64-48, Lampoldshausen, Germany, June 1964.

[3]Miyajima, H., and Nakahashi, K., "Low-Thrust Engine Performance with a 300:1 Nozzle," AIAA Paper 83-1313, June 1983.

[4]Braitinger, M., Ruppe, H. O., and Schmucker, R. H., "Aspekte zur Leistungsvorhersage von chemischen Raketentriebwerken," RT-TB 78/3, DGLR Jahrestagung, Darmstadt, Germany, Sept. 1978.

[5]Rao, G. V. R., "Exhaust Nozzle Contour for Optimum Thrust," *Jet Propulsion*, June 1958.

[6]Koelle, H. H., *Handbook of Astronautical Engineering*, McGraw–Hill, New York, 1962.

[7]Gordon, S., and McBride, B. J., "Computer Program for Calculation of Complex Chemical Equilibrium Compositions, Rocket Performance," NASA-SP-273, March 1976.

[8]Nickerson, G. R., Dang, L. D., and Coats, D. E., "Two-Dimensional Reference Computer Program," NAS 8-35931, Huntsville, AL, April 1985.

[9]Hagemann, G., and Manski, D., "Parametrische Untersuchungen der Verlusteffekte von Raketendüsen," DGLR-92-03-048, Bonn, Germany, Oct. 1992.

[10]Jung, W., and Manski, D., "Parameteranalyse mit SYS—Benutzeranleitung," DLR-IB-643-90/20, Lampoldshausen, Germany, Dec. 1990.

[11]Anderson, J. D., *Hypersonic and High Temperature Gas Dynamics*, McGraw–Hill, New York, 1990.

[12]Zucrow, M. J., and Hoffman, J. D., *Gas Dynamics*, Wiley, New York, 1977.

[13]Nickerson, G. R., and Dang, L. D., "Performance Prediction for an SSME Configuration with an Enlarged Throat," NASA-CR-178740, Nov. 1986.

[14]Kirner, E., Oechslein, W., Thelemann, D., and Wolf, D., "Development Status of the Vulcain (HM60) Thrust Chamber," AIAA Paper 90-2255, July 1990.

[15]Stohler, S. L., "SSME Update," AIAA Paper 89-2409, July 1989.